JOURNAL OF GEOPHYSICAL RESEARCH, VOL. 113, D06102, doi:10.1029/2007JD009176, 2008

Strong sensitivity of late 21st century climate to projected changes in short-lived air pollutants

Hiram Levy II,[1] M. Daniel Schwarzkopf,[1] Larry Horowitz,[1] V. Ramaswamy,[1] and K. L. Findell[1]

Received 11 July 2007; revised 25 September 2007; accepted 10 December 2007; published 19 March 2008.

[1] This study examines the impact of projected changes (A1B "marker" scenario) in emissions of four short-lived air pollutants (ozone, black carbon, organic carbon, and sulfate) on future climate. Through year 2030, simulated climate is only weakly dependent on the projected levels of short-lived air pollutants, primarily the result of a near cancellation of their global net radiative forcing. However, by year 2100, the projected decrease in sulfate aerosol (driven by a 65% reduction in global sulfur dioxide emissions) and the projected increase in black carbon aerosol (driven by a 100% increase in its global emissions) contribute a significant portion of the simulated A1B surface air warming relative to the year 2000: 0.2°C (Southern Hemisphere), 0.4°C globally, 0.6°C (Northern Hemisphere), 1.5–3°C (wintertime Arctic), and 1.5–2°C (~40% of the total) in the summertime United States. These projected changes are also responsible for a significant decrease in central United States late summer root zone soil water and precipitation. By year 2100, changes in short-lived air pollutants produce a global average increase in radiative forcing of ~1 W/m^2; over east Asia it exceeds 5 W/m^2. However, the resulting regional patterns of surface temperature warming do not follow the regional patterns of changes in short-lived species emissions, tropospheric loadings, or radiative forcing (global pattern correlation coefficient of −0.172). Rather, the regional patterns of warming from short-lived species are similar to the patterns for well-mixed greenhouse gases (global pattern correlation coefficient of 0.8) with the strongest warming occurring over the summer continental United States, Mediterranean Sea, and southern Europe and over the winter Arctic.

Citation: Levy, H., II, M. D. Schwarzkopf, L. Horowitz, V. Ramaswamy, and K. L. Findell (2008), Strong sensitivity of late 21st century climate to projected changes in short-lived air pollutants, *J. Geophys. Res.*, *113*, D06102, doi:10.1029/2007JD009176.

1. Introduction

[2] The impact of short-lived species on climate was first discussed in the 1970s when it was argued that anthropogenic aerosols were responsible for the global cooling then being observed [e.g., *Bryson and Dittberner*, 1976], but this view was soon replaced by concerns over carbon dioxide (CO_2)-driven global warming. Short histories of our developing understanding of the climate role for short-lived species are provided by *Ramaswamy et al.* [2001] and *Forster et al.* [2007] and they are summarized below.

[3] The climate impacts of tropospheric ozone and sulfate aerosols were noted and sulfate aerosols' indirect effects on clouds acknowledged by *Shine et al.* [1990]. *Shine et al.* [1995] presented the first anthropogenic radiative forcing (RF) bar chart comparing changes from preindustrial to present. The bar chart for present-day RF was broken into aerosol components (sulfate, fossil-fuel soot, and biomass burning aerosols) with a separate range for indirect effects [*Schimel et al.*, 1996]. By the end of the 1990s, *Ramaswamy et al.* [2001] included individual present-day radiative forcings for all anthropogenic aerosols, including direct and indirect effects and tropospheric and stratospheric ozone. *Forster et al.* [2007] further refined the present-day radiative forcing by anthropogenic short-lived species is further refined.

[4] Recent atmosphere-ocean general circulation model (AOGCM) studies of anthropogenic and volcanic sulfate have also demonstrated that these scattering aerosols have reduced the current global warming of surface atmospheric temperature [*Brasseur and Roeckner*, 2005] and ocean temperature [*Delworth et al.*, 2006]. However, while the Intergovernmental Panel on Climate Change (IPCC) process and other recent research have directed considerable effort toward quantifying the past and present anthropogenic contributions of short-lived species to current radiative forcing and climate change, there has been much less emphasis on the future role of short-lived species emissions. *Hansen et al.* [2000] have argued that reductions in emissions of ozone precursors and black carbon (BC) aerosol

[1]Geophysical Fluid Dynamics Laboratory, NOAA, Princeton University, Princeton, New Jersey, USA.

would significantly reduce the warming over the next 50 years.

[5] In this study we employ the A1B "marker" emission scenario, an IPCC scenario that includes either explicit or implicit projections for emissions of short-lived species and generates a middle-of-the-road radiative forcing. With a series of 100-year simulations, we assess the sign, magnitude, and temporal trend of future climate change due to the projected changes in short-lived radiative species of anthropogenic origin: tropospheric ozone, black carbon, sulfate, and organic carbon. While these short-lived air pollutants may be important contributors to future radiative forcing and climate change, their control is currently driven by local and regional air quality issues.

[6] Our simulations focus on the changes in aerosol and ozone concentrations resulting from changes in anthropogenic emissions, but they exclude feedbacks from climate change on emissions, chemical processing, or removal rates of these species [e.g., *Zeng and Pyle*, 2003; *Stevenson et al.*, 2005; *Brasseur et al.*, 2006; *Liao et al.*, 2006]. Methane itself is specified as a well-mixed greenhouse gas whose global concentration follows the A1B scenario in both our simulations of climate and our calculations of short-lived species concentrations. This precludes any chemical feedbacks on methane concentrations via changes in atmospheric oxidant levels and methane lifetime [*Wild et al.*, 2001; *Fiore et al.*, 2002].

2. Experimental Design

2.1. Emission Scenarios

[7] In this study we employ two emission scenarios: A1B and A1B*. We choose the A1B scenario because its radiative forcing at 2100 is in the middle of the four scenarios discussed by the *Intergovernmental Panel on Climate Change (IPCC)* [2007b] and has been the most extensively studied. The A1B scenario is the complete A1B marker emission scenario [*Nakicenovic and Swart*, 2000]. This includes projected concentrations of well-mixed greenhouse gases as well as future emissions of precursors to tropospheric ozone and sulfate aerosol and direct emissions of black and organic carbon (OC) aerosol (see sections 2.2 and 2.4 of *Horowitz* [2006] for emission details). These emissions are based on projections of technological change, economic and population growth, and regulatory action out to 2100. The second scenario, A1B*, has the same concentrations as A1B for the well mixed greenhouse gases, but the four anthropogenic short-lived species distributions (tropospheric ozone, sulfate aerosol, and black and organic carbon aerosols) were fixed at their 2001 monthly values [*Horowitz*, 2006].

[8] The well-mixed greenhouse gas concentrations used in both the A1B and A1B* scenarios are given in Figure 1a. By 2100, CO_2 has increased continuously from a present level of 380 to more than 715 ppm while nitrous oxide (N_2O) has increased from 315 to 370 ppb. Methane (CH_4) increases from a present level of 1.75 to a maximum of 2.4 ppm by 2050 and then decreases to 2.0 ppm by 2100. The A1B marker emissions for the short-lived species are discussed in detail by *Horowitz* [2006] and their global emission totals are given in Figures 1b–1d. Emissions of nitrogen oxides (NO_x), the primary tropospheric ozone precursor, increase by 40% until 2030 and then slowly decrease while still remaining above the 2000 value. BC and OC emissions, which are scaled to carbon monoxide (CO) emissions, increase continuously and almost double by 2100. Global emissions of sulfur dioxide (SO_2), the precursor of sulfate aerosol, increase by 35% until 2020 and then decrease rapidly afterward, reaching ~35% of 2000 levels by 2100.

[9] The global chemical transport model Model for Ozone and Related Chemical Tracers version 2.4 (MOZART-2), which has been described in detail previously [*Horowitz et al.*, 2003; *Tie et al.*, 2005] is used to generate the ozone, sulfate, and black and organic carbon distributions resulting from the emission scenarios discussed above and described by *Horowitz* [2006]. MOZART-2 includes 63 gas phase species; 11 aerosol and precursor species to simulate sulfate, nitrate, ammonium, and black and organic carbon; and 5 size bins for mineral dust. It is driven by meteorological inputs every 3 h from the middle atmosphere version of the National Center for Atmospheric Research Community Climate Model [*Kiehl et al.*, 1998]. The horizontal resolution is 2.8° latitude by 2.8° longitude, with 34 hybrid sigma pressure levels extending up to 4 hPa. Simulations were performed as 2-year snapshots each decade with anthropogenic emissions evolving according to the IPCC Special Report on Emissions Scenarios (SRES) A1B marker scenario [*Horowitz*, 2006]. The meteorology was the same for each decade, thus excluding any feedbacks from climate change on natural emissions and rates of chemical reactions and removal. Stratospheric ozone in the MOZART simulations was held constant at present-day levels. Emissions and initial conditions for methane were scaled each decade to match the global average methane abundances specified in the A1B marker scenario.

[10] A recent evaluation by *Ginoux et al.* [2006] of the present-day aerosol distributions and optical depths used in this study [*Horowitz*, 2006] found: (1)The predicted aerosol concentrations are within a factor of 2 of the observed values with a tendency to be overestimated; (2) The modeled and satellite-observed global mean optical depths agree within 10%, though this masks significant regional differences; (3) The largest discrepancies in optical depth are over the northeastern United States (too high) and the biomass burning regions and the southern oceans (too low); (4) Globally, the excessive optical depth from sulfate aerosols compensates for underestimates in organic and sea-salt aerosol contributions.

[11] All natural aerosol distributions (sea salt, dust, volcanic, and other natural sulfate contributions), as well as the distributions of vegetation, are held constant at the same values for both the A1B and A1B* scenarios [*Haywood et al.*, 1999; *Horowitz*, 2006]. Stratospheric ozone in the A1B simulation is held at year 2000 levels through 2010, restored linearly to 1979 values by 2050, and then held constant through 2100. Stratospheric and tropospheric ozone values are merged at the tropopause.

2.2. Tropospheric Loading of Short-Lived Species

[12] In Figure 2 we present the latitude-longitude maps of the year 2000 tropospheric column loading for the three primary short-lived radiative forcing agents, sulfate aerosol,

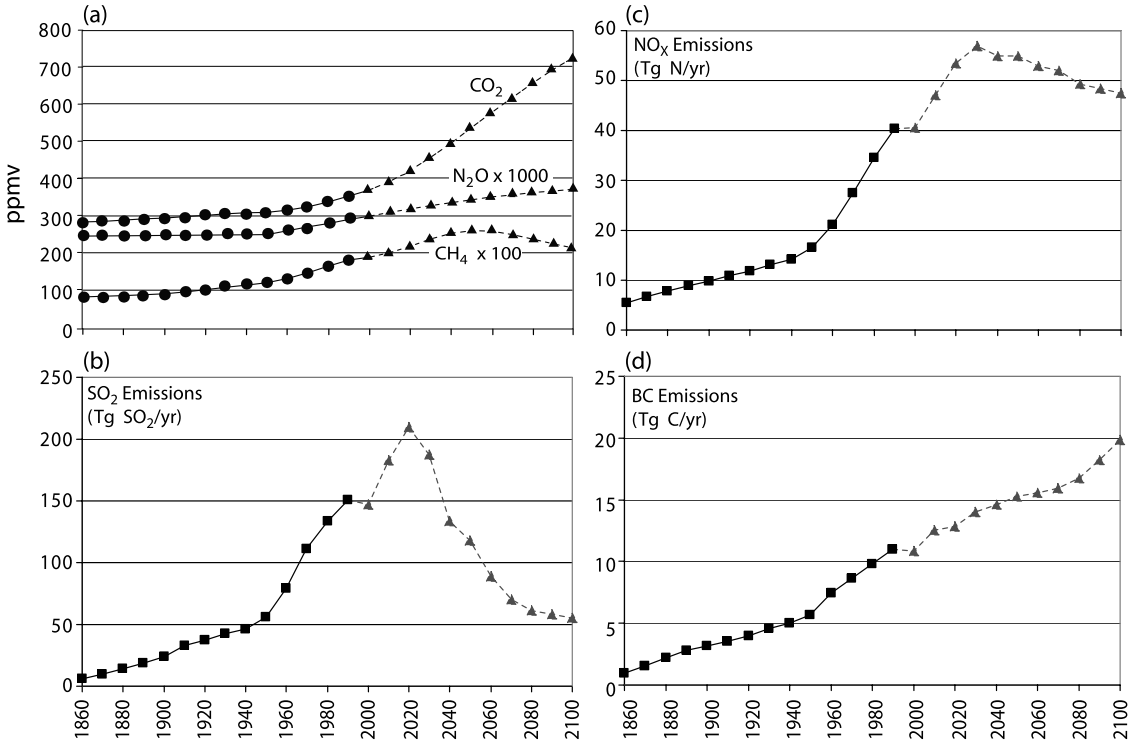

Figure 1. (a) Concentration time series of well-mixed greenhouse gases for the historical (1860–2000) period (solid lines with circles) and for the SRES A1B emission scenario [*Nakicenovic and Swart*, 2000] between 2000 and 2100 (dashed lines with triangles). (b) Sulfur dioxide (SO_2), (c) nitrogen oxides (NO_x), and (d) black carbon (BC) emissions for the historical (1860–2000) period (solid lines with squares) and for the SRES A1B marker emission scenario [*Nakicenovic and Swart*, 2000] between 2000 and 2100 (dashed lines with triangles).

black carbon aerosol, and ozone along with changes in their loading from the years 2000 to 2030 and 2100. These were all generated by *Horowitz* [2006] using the A1B marker scenario in MOZART-2.

[13] The most dramatic changes are projected for the sulfate and BC aerosol loadings. The current sulfate loading (Figure 2a) is dominated by the major industrial regions: United States, Europe, and south and east Asia. By 2030 (Figure 2b) the global atmospheric load reaches a maximum with a significant increase over Asia and the North Pacific driven by the large increases in emissions from south and east Asia and modest increases over the South Atlantic and Indian oceans driven by increased emissions from South America and southern Africa. There are already modest reductions over the United States and Europe. By 2100 (Figure 2c) the global sulfate load has decreased by 40% relative to 2000, predominately in the Northern Hemisphere and particularly over east Asia. The BC load shown in Figures 2d–2f is projected to increase continuously throughout the 21st century. Currently, (Figure 2d) the maximum loadings are over the major present-day source regions: North America and Europe (primarily fossil fuel), South America and Africa (primarily biomass burning), and south and east Asia (fossil fuel, biomass, and biofuel burning). By 2100 (Figure 2f), the global load has grown by 80% with the increase primarily over south and east Asia.

[14] Tropospheric ozone column loading in Figures 2g–2i is strongly influenced by NO_x emissions. The present ozone loading (Figure 2g) has a significant south-to-north gradient, but, because of a relatively long atmospheric lifetime and significant tropospheric background, the south-to-north gradient is much less and its distribution is much more zonal than either sulfate or BC. The projected increase throughout the 21st century (Figures 2h and 2i) is relatively modest with a maximum increase (15–25%) in a tropical belt stretching from the major biomass burning areas of South America and Africa through south Asia due to modest increases in background methane (see Figure 1a) and regional NO_x emissions.

[15] By 2100, the A1B marker scenario projects a (40%) decrease in the global burden of sulfate, a (80%) increase in BC's global burden, and a modest (13%) increase in tropospheric ozone's global column loading. Each of these will result in positive radiative forcing changes (i.e., heating), as discussed in section 2.3. The tropospheric loading changes, particularly in sulfate and BC, are overwhelmingly in the Northern Hemisphere, highly regional, and predominately in south and east Asia with more modest contributions over the United States and Europe.

2.3. Radiative Forcing

[16] Before examining the full climate response to these changes in ozone, sulfate, BC, and OC loadings, it is instructive to consider the evolution of the radiative forcing due to these loading changes throughout the 21st century.

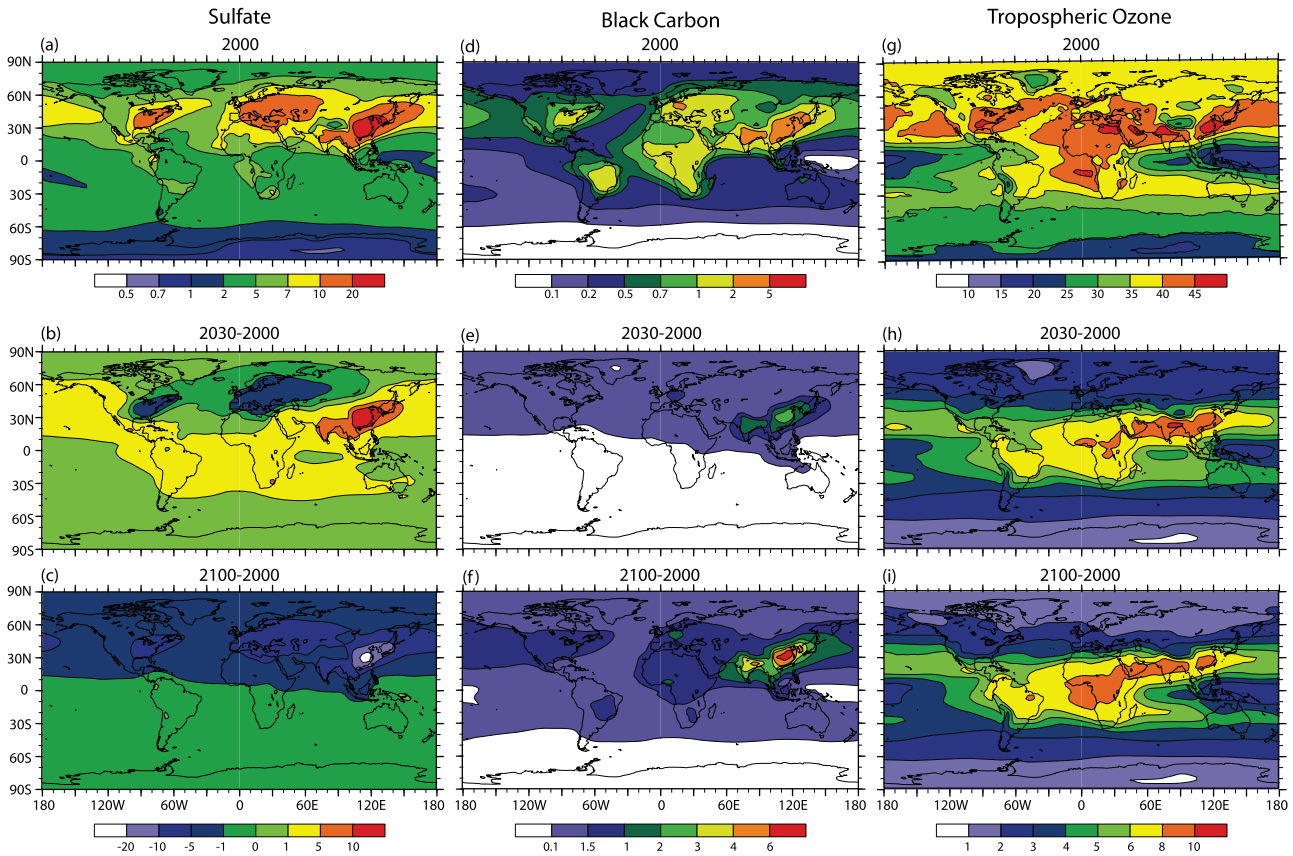

Figure 2. Latitude-longitude maps of the year 2000 tropospheric column loading along with the changes in loadings for years 2030 and 2100 using the A1B marker scenario relative to year 2000 for the three primary short-lived radiative forcing agents: (a–c) sulfate aerosol (in $mgSO_4/m^2$), (d–f) black carbon aerosol (in mgC/m^2), and (g–i) tropospheric ozone (in Dobson Units (DU)).

Radiative forcing, first calculated by *Wetherald and Manabe* [1980] for the top of the model atmosphere, is defined in the IPCC studies [e.g., *Ramaswamy et al.*, 2001] as the change in net (down minus up) irradiance (solar plus longwave, in W/m^2) at the tropopause after allowing for stratospheric temperatures to readjust to radiative equilibrium but with surface and tropospheric temperatures and state held fixed at the unperturbed values. Radiative forcing is used to assess and compare the anthropogenic and natural drivers of climate change. It is a simple measure for both quantifying and ranking the many different influences on climate change; it provides a limited measure of climate change as it neglects feedbacks and does not attempt to represent the overall climate response [*Ramaswamy et al.*, 2001].

[17] Here we compute the annual mean-adjusted radiative forcing using atmospheric profiles from the unforced (i.e., preindustrial) coupled ocean-land-atmospheric model at equilibrium for the 15th day of each month but with the forcing agents specified at year 2000, 2030, 2050, or 2100 values. The radiation algorithm is the same as in the climate model described in section 2.4 [*Knutson et al.*, 2006]. The tropopause is set at 100 hPa at the equator and descends linearly in latitude to 300 hPa at either pole. Note that in these calculations and in the actual climate simulations we only consider direct radiative forcing for aerosols. The aerosol optical properties are specified according to *Haywood et al.* [1999]. The sulfate optical properties do vary with relative humidity. The radiation algorithm neglects the effects of aerosol scattering in the infrared.

[18] The annual mean global and hemispheric forcings for A1B, A1B* (change in well-mixed greenhouse gases only), and the individual forcing agents are shown in Table 1. While the net global radiative forcing due to short-lived species is almost zero at year 2030 relative to 2000, it contributes ~19% of the positive change by 2050. By 2100, they (primarily decreasing sulfate and increasing BC aerosol) contribute ~26% of the global change and ~36% of the Northern Hemisphere change. The contributions from tropospheric ozone and OC aerosol are relatively modest and tend to offset. The near zero radiative forcing change due to short-lived species for year 2030 does not appear to be strongly scenario dependent, since quite different alternative A1B scenarios also produce similar results for 2030. However, the strong warming contribution from short-lived species by year 2100 is scenario dependent (see discussion by *Shindell et al.* [2008]).

[19] It is interesting to note that the *IPCC* [2001] annual mean global radiative forcing change for 2100 (also shown in Table 1) is within 8% of the well-mixed greenhouse gases value used in this study and that the total change is also similar (within 5%), while the individual aerosol contributions are significantly different. Most of this difference is cancelled by the ~0.6 W/m^2 increase because of indirect aerosol effects included in the IPCC calculation.

Table 1. Adjusted Radiative Forcing[a]

	Component (2030–2000)			Component (2050–2000)			Component (2100–2000)			
	Global	NH	SH	Global	NH	SH	Global	NH	SH	IPCC[b]
All Forcing	1.23	1.34	1.12	2.50	3.11	1.89	4.52	5.24	3.79	4.72[c]
Well-Mixed Greenhouse Gases	1.19	1.19	1.20	2.02	2.01	2.03	3.35	3.34	3.36	3.62
A1B–A1B* (All Short-Lived Species)	0.04	0.15	−0.08	0.48	1.10	−0.14	1.17	1.91	0.42	0.31
BC	0.21	0.38	0.04	0.30	0.53	0.07	0.63	1.02	0.25	0.31
OC	−0.04	−0.07	−0.01	−0.06	−0.10	−0.02	−0.15	−0.22	−0.09	−0.38
Sulfate[d]	−0.32	−0.36	−0.29	0.01	0.43	−0.40	0.51	0.93	0.08	0.24
Total Aerosol	−0.15	−0.05	−0.26	0.24	0.85	−0.36	0.98	1.71	0.24	0.17
Ozone	0.19	0.20	0.18	0.23	0.25	0.21	0.19	0.19	0.18	0.14

[a]In W/m^2.
[b]Appendix II [*IPCC*, 2001].
[c]This includes a crude treatment of indirect aerosol effects.
[d]Sulfate aerosol produces a negative radiative forcing. However, if there is a significant decrease in sulfate aerosol as the A1B scenario projects for 2100, the net change in 2100 radiative forcing relative to 2000 for sulfate aerosol will be positive (i.e., a reduction in sulfate aerosol reduces its negative radiative forcing, which is, in the net, an increase).

[20] We next consider the regional distribution of the year 2100 changes in radiative forcing (Figure 3). The total change (Figure 3a) is positive everywhere, relatively uniformly distributed zonally, and increasing from south to north with a northern midlatitude maximum and a hot spot (>13 W/m^2) over east Asia. The 2100 change due to only the short-lived species (Figure 3b) shows the source of both the northern midlatitude maximum and the hot spot over east Asia. There is very little contribution in the Southern Hemisphere (SH), with the exception of modest forcings over tropical Africa and South America.

[21] Examining the radiative forcing from changes in the two principal species, sulfate and BC aerosol (Figures 3c and 3d), we confirm their role as sources of both the northern midlatitude maximum and east Asian hot spot. Comparing Figures 3b–3d with the year 2100 changes in tropospheric loadings in Figures 2c and 2f, it is clear that the radiative forcing regional patterns and the total column changes for sulfate and BC aerosols are similar.

2.4. Geophysical Fluid Dynamics Laboratory Climate Model

[22] We estimate the climate response to changes in well-mixed greenhouse gases and short-lived species using the NOAA/Geophysical Fluid Dynamics Laboratory (GFDL) coupled climate model (the AOGCM). Its formulation and

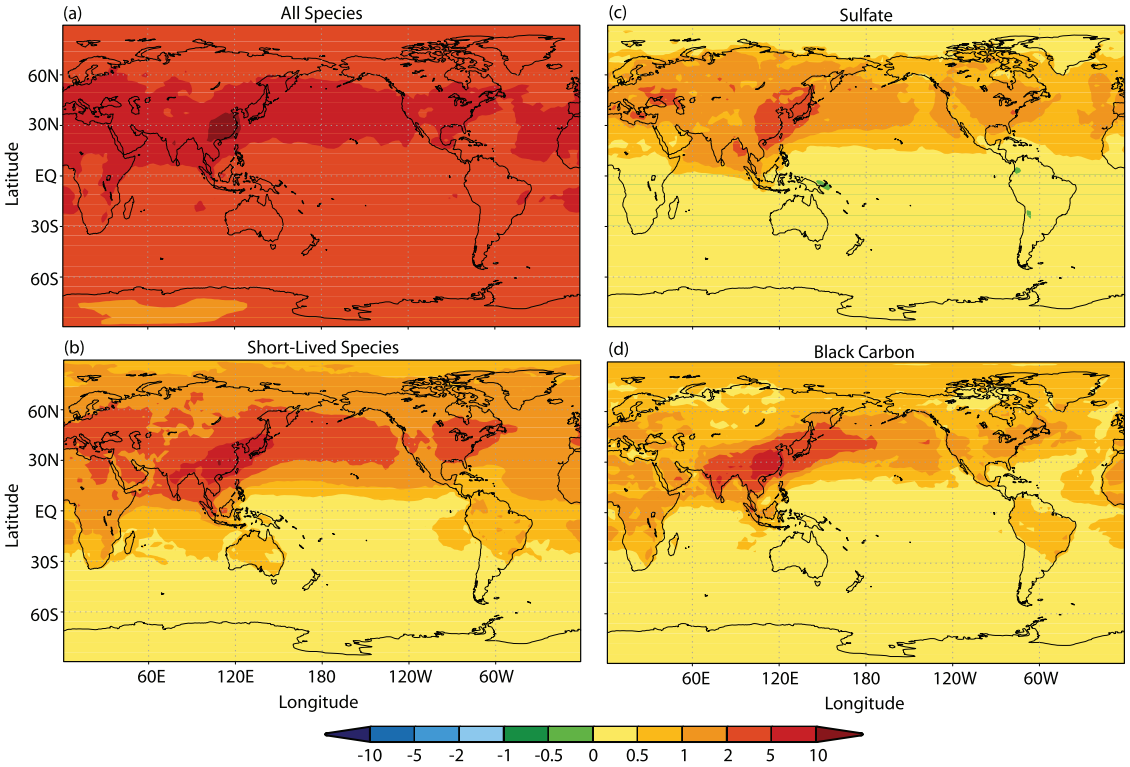

Figure 3. Latitude-longitude maps of changes in annual mean-adjusted radiative forcing (W/m^2) between years 2100 and 2000 for the (a) total forcing (well-mixed greenhouse gases plus short-lived species), (b) contribution from short-lived species only, for (c) the contribution from sulfate aerosol, and (d) contribution from black carbon aerosol.

simulation characteristics have been previously described in detail [*Delworth et al.*, 2006], which we summarize here. The model simulates atmospheric and oceanic climate and variability from the diurnal timescale through multicentury climate change without employing flux adjustment. The resolution of the land and atmospheric components is 2.5° longitude by 2° latitude and the atmospheric model has 24 vertical levels. The ocean resolution is 1° in latitude and longitude, with meridional resolution equatorward of 30° becoming progressively finer, such that the meridional resolution is 1/3° at the equator. There are 50 vertical levels in the ocean, with 22 evenly spaced levels within the top 220 m. The ocean component has poles over North America and Eurasia to avoid polar filtering.

[23] The control simulation has a stable, realistic climate when integrated over multiple centuries and a realistic El Niño–Southern Oscillation [*Wittenberg et al.*, 2006]. Its equilibrium climate response to a doubling of CO_2 is 3.4°C [*Stouffer et al.*, 2006]. Using a five-member ensemble simulation of the historical climate (1861–2003), including the evolution of natural and anthropogenic forcing agents, the GFDL AOGCM is able to capture the global historical trend in observed surface temperature for the 20th century as well as many continental-scale features [*Knutson et al.*, 2006]. However, the model shows some tendency for too much 20th century warming in lower latitudes and too little warming in higher latitudes. Differences in Arctic Oscillation behavior between the model and observations contribute substantially to an underprediction of the observed warming over northern Asia. El Niño interactions complicate comparisons of observed and simulated temperature records for the El Chichón and Mount Pinatubo eruptions during the early 1980s and early 1990s [*Knutson et al.*, 2006]. In Figure 7d of *Knutson et al.* [2006], where the model ensemble and observations are compared grid box by grid box, ~60% of those grid boxes with sufficient observational data have 20th century surface temperature trends that agree quantitatively with the model ensemble. In general, many observed continental-scale features, including a 20th century cooling over the North Atlantic, are captured by the model ensemble, as Figures 7a and 7c of *Knutson et al.* [2006] show. However, the model ensemble does not capture the observed cooling over the southeastern United States and it produces a 20th century cooling over the North Pacific that is not observed.

[24] In this study, transient integrations over both the A1B and A1B* scenarios were performed for ensembles of three members for the period (2001–2100). The respective starting points of these integrations were the atmospheric states on 1 January 2001 of each of the three historical climate simulations. The A1B* scenario uses 2001 monthly values for the distribution of short-lived species throughout the integration, while A1B uses the monthly mean distributions generated from the A1B marker emission scenarios where short-lived species values vary throughout the 21st century. To determine the contribution of the projected changes in the short-lived species to climate change, the averages of the three-member ensemble employing the A1B* scenario were subtracted from the averages of the three-member ensemble employing the full A1B scenario. The monthly average short-lived species loadings were calculated for 10-year time slices with MOZART-2 and interpolated linearly. Indirect effects of the aerosols on clouds and precipitation were not included in the climate simulations.

3. Results and Discussion

[25] In this section we examine the impact of the changing concentrations of tropospheric ozone, sulfate aerosol, and black and organic carbon aerosol on the surface temperature, precipitation, and soil moisture.

3.1. Surface Temperature

[26] In Figures 4a and 4b we plot time series of global average surface temperature anomalies relative to year 2001 for both A1B and A1B* scenarios where the shaded areas represent the range of the three independent members of each ensemble. In the 2nd half of the 21st century the two scenarios begin to diverge noticeably. This is confirmed in Figure 4c where we show the difference between Figures 4a and 4b which is the warming due only to the changing levels of short-lived species. The shaded area about the global average temperature difference represents the range of the differences between the three independent pairs from the two ensembles. While by year 2100 the average impact in the SH is still quite modest, as we might expect from their small radiative forcing in Figure 3c, the contributions of changes in short-lived species to the global temperature difference (0.4–0.5°C) and Northern Hemisphere (NH) temperature difference (0.6–0.7°C) are obvious.

[27] The small negative surface temperature signal (A1B – A1B*) out to 2030 is consistent with the increasing sulfate aerosol concentrations (Figure 2b), which increase the scattering of incoming solar radiation, thereby reducing the radiative forcing in the full A1B scenario and causing cooling. The transition in the surface temperature between 2030 and 2050 is consistent with the abrupt decrease in sulfate aerosol loading (Figures 2b and 2c), resulting in a decrease in cooling because of sulfate aerosols. There is a hint of a developing impact in the SH near 2100, but another 50–100 years of integration would be needed to see if this is due to the change in short-lived species, which occurs primarily in the NH, or just the result of natural climate variability in the SH.

[28] We next examine the regional nature of the climate response in Figures 5 and 6 and focus on a 10-year average (2091–2100) at the end of the 21st century where the time series have already shown the largest impact from short-lived species. For the annual, winter (DJF), and summer (JJA) average temperature changes (Figures 5c, 6c, and 6f, respectively), we determine the regions of statistical significance (at 95% confidence level) by comparing, for each grid box, the 2001–2100 time series for the short-lived species (A1B(t) − A1B*(t)) to a 1000-year time series of the GFDL climate model control (unforced) simulation.

[29] In Figure 5 we compare the annual surface temperature warming for the full A1B scenario between the 2090s (2091–2100) and the 2000s (2001–2010) with the corresponding contributions to annual global warming from the projected increasing well-mixed greenhouse gases and from the projected changes in short-lived species emissions. The large-scale patterns, particularly in the NH, are similar in all three panels with a significant land-sea contrast (most

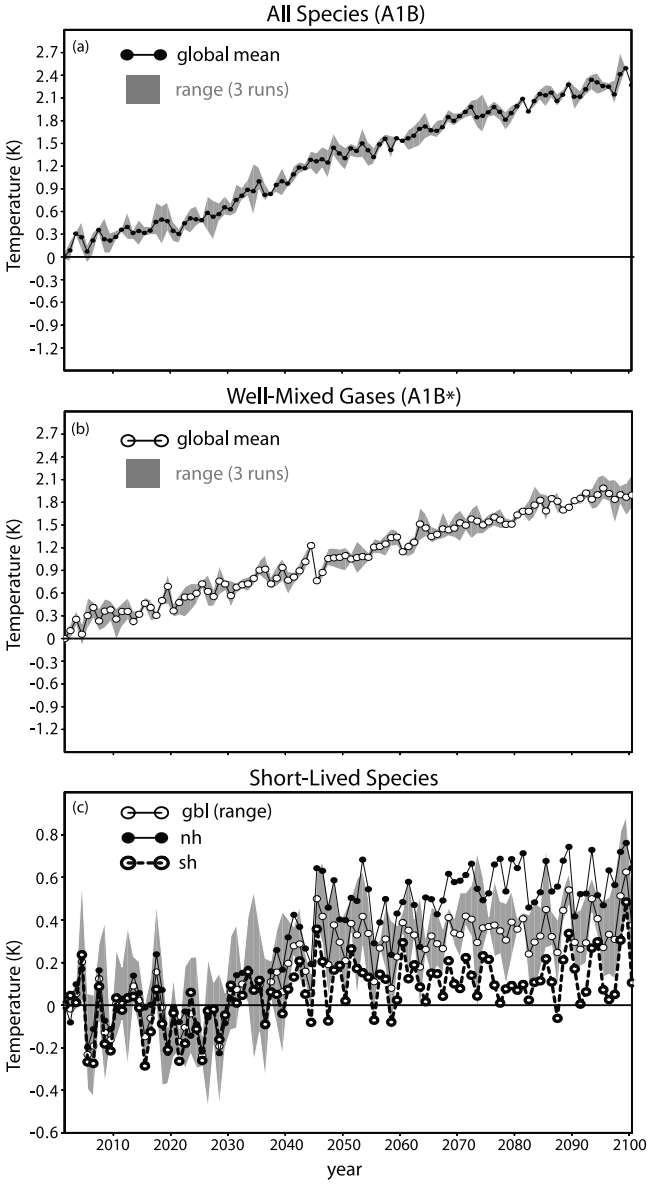

Figure 4. Time series of global annual-mean surface air temperature change from 2001 for (a) all greenhouse gases and aerosols (A1B scenario); (b) the well-mixed greenhouse gases only (A1B* scenario); and (c) the global, Northern Hemisphere, and Southern Hemisphere average surface temperature change due to the change in short-lived species only (A1B − A1B*). The shaded areas in Figures 4a and 4b represent the range of the three independent members of each ensemble, and the shaded area in Figure 4c represents the range of the three pairs for the global average surface temperature.

of the warming in the NH and most of that over midlatitude landmasses and the Arctic). For most of the NH, the warming due only to short-lived species (Figure 5c) is statistically significant at the 95% confidence level. We note that the general pattern of warming observed in Figure 5a is also found in the 18 models simulating climate for the full A1B scenario by the *IPCC* [2007a, Figure SPM-5] and *Meehl et al.* [2007, Figure 10.8]. Note that two boxes have been drawn over North America in Figure 5a. The larger box is the United States box that is considered in Figure 7 and has the boundaries (30–50°N and 125–70°W). The small box is the central United States box with the boundaries (32.5–45°N and 105–82.5°W) that is used in Figure 9.

[30] Referring back to Figure 3b, we note that for the year 2100 changes in short-lived species, regional patterns of radiative forcing are very different from the warming patterns in Figure 5c. This is confirmed by a global pattern correlation coefficient of −0.172. We next consider the similarity in the temperature change (primarily warming) patterns for all 3 panels in Figures 5a–5c. The global pattern correlation coefficient for Figures 5a and 5b is 0.96 and 0.83 for Figures 5a and 5c. This lack of correlation between regional patterns of radiative forcing and the resulting patterns of surface temperature change as well as the similarity of a particular climate model's surface temperature response to different radiative forcing patterns have all been noted and discussed previously [e.g., *Forster et al.*, 2000; *Mitchell et al.*, 2001; *Boer and Yu*, 2003]. We believe that these results and the earlier studies strongly suggest that the short-lived species regional pattern of temperature change in Figure 5c is due primarily to the regional pattern of the model's climate response and is not significantly influenced by the regional radiative forcing pattern resulting from their changing tropospheric loadings. However, the specific mechanism or mechanisms responsible, be they dynamical, local feedback processes, or some combination thereof, are not yet clearly established. To make a more definitive statement, additional sensitivity tests employing a range of radiative forcings with different spatial distributions are needed.

[31] In Figure 6 we compare the seasonal surface temperature responses between the 2090s and 2000s resulting from the full A1B scenario, increased well-mixed greenhouse gases, and projected changes in short-lived species emissions. Again the large-scale climate response patterns (a significant land-sea contrast in warming, much less warming in the SH, the greatest DJF warming in the high latitudes and the greatest JJA warming over the United States and southern Europe) are common to all three panels (full A1B, well-mixed greenhouse gases, and short-lived species). While much of the DJF warming in the NH in Figure 6c is significant at the 95% confidence level, the largest warming over Canada as well as the warming over Siberia is not significant because of high interannual variability. Almost all the JJA warming across the NH subtropics and midlatitudes, including the maxima in warming over the United States and southern Europe, is statistically significant at the 95% confidence level in Figure 6f. In neither season are the temperature changes in the SH due to changes in short-lived species significant. Again we note that the multimodel mean from the *IPCC* [2007a] and *Meehl et al.* [2007, Figure 10.9] shows similar seasonal 2100 climate responses for the full A1B scenario.

[32] We next compare the climate response patterns for the winter and summer. The global DJF pattern correlation coefficient in Figures 6a–6c for full A1B and well-mixed greenhouse gases is 0.97 and for full A1B and short-lived species is 0.80. The JJA global pattern correlation coefficient in Figures 6d–6f for full A1B and well-mixed greenhouse gases is 0.91 and for full A1B and short-lived

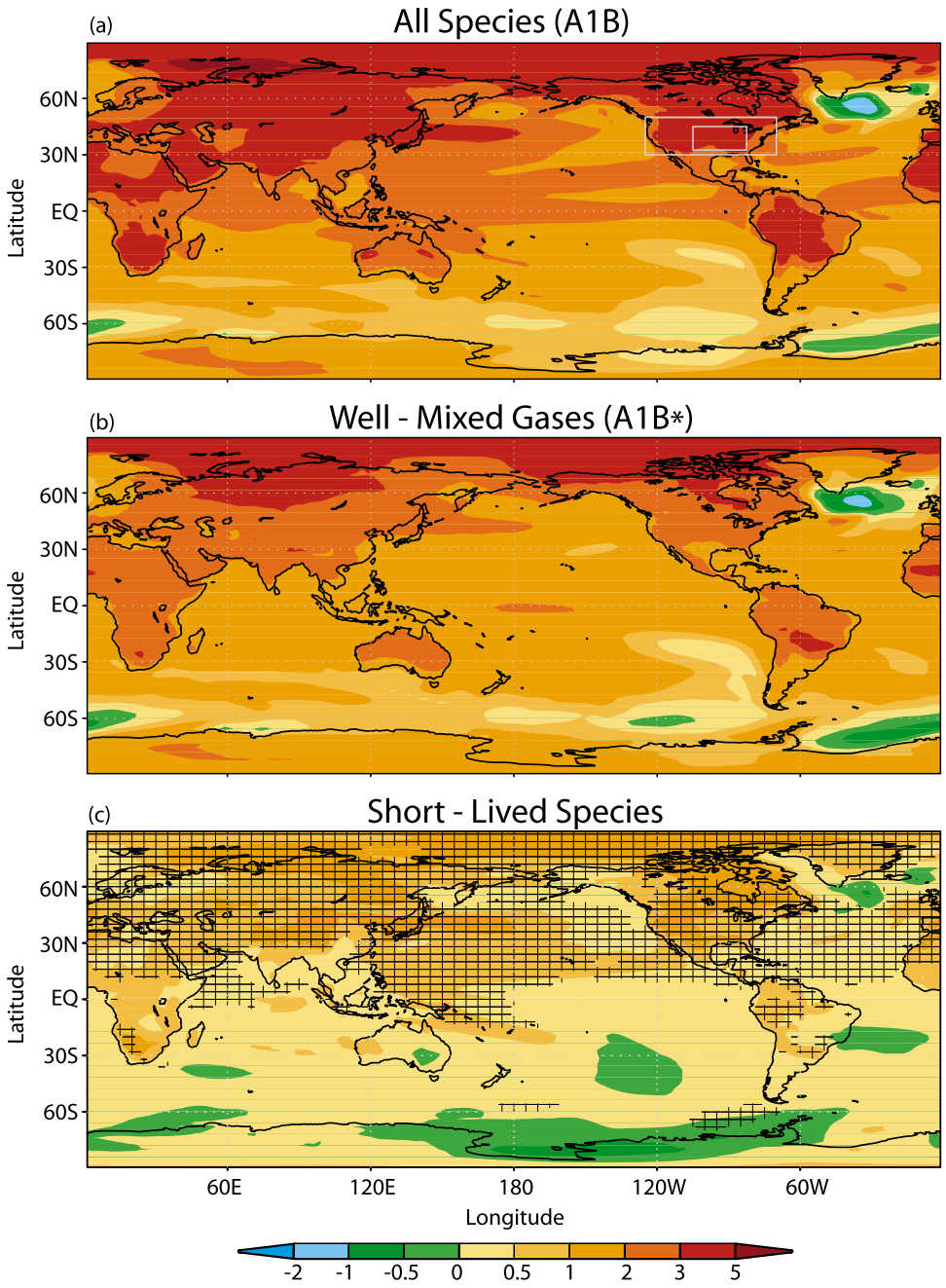

Figure 5. Latitude-longitude maps of annual surface air temperature change (°K) from the 2000s (years 2001–2010) to the 2090s (years 2091–2100) for the (a) full A1B scenario (A1B(2090s) − A1B(2000s)), (b) forcing by the well-mixed greenhouse gases only (A1B*(2090s) − A1B*(2000s)), and (c) forcing only by the short-lived species (A1B(2090s) − A1B*(2090s)) − (A1B(2000s) − A1B*(2000s)). Hatched areas in Figure 5c denote regions where the temperature change is significant at the 95% confidence level. The larger box in Figure 5a contains the continental United States region used in Figure 7 and the smaller box contains the central United States region examined in Figure 9.

species is 0.76. As for the annual response patterns, we see that the seasonal warming patterns are highly correlated. We see this as further support for our argument that the patterns of climate responses are the result of the AOGCM's regional climate response not a direct localized response to radiative forcing patterns.

[33] In Figure 7 we now focus on the large summertime warming over the United States first seen in Figure 6f. The area considered is shown as the large box drawn in Figure 5a. The United States time series shows an average surface temperature warming of ~4°K for the A1B scenario by year 2100 with a contribution of ~1.5°K from the change in short-lived species. Throughout the 21st century, we note the significant role played by regional interannual variability in the large year-to-year excursions of 1°C or more for the full A1B forcing. With net global radiative forcing due

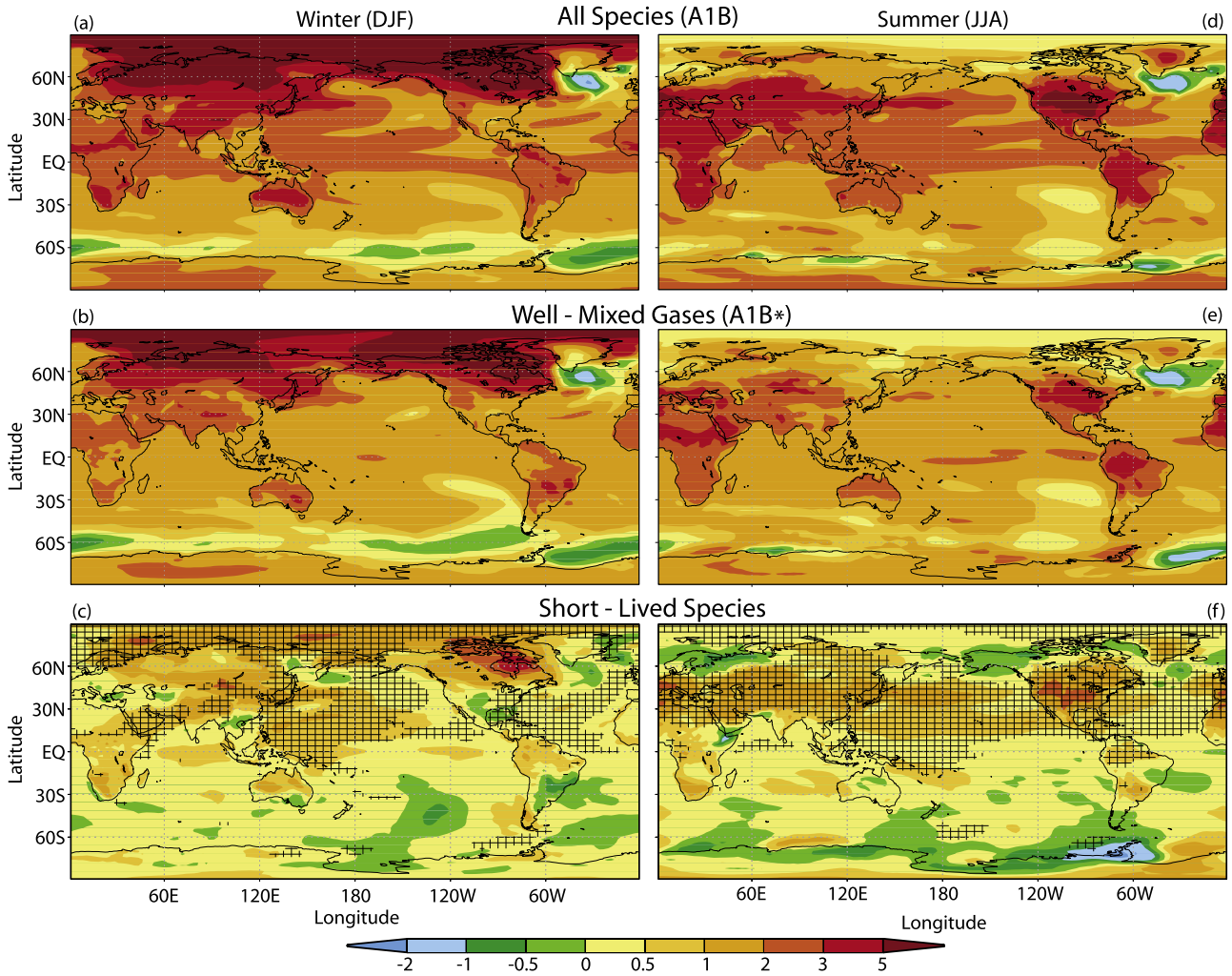

Figure 6. Same as for Figure 5 except that they are for winter (DJF) temperature changes (°K) for the (a) A1B scenario, (b) A1B* scenario, and (c) short-lived species and for summer (JJA) temperature changes (°K) for the (d) A1B scenario, (e) A1B* scenario, and (f) short-lived species.

to short-lived species almost zero through 2030 (see Table 1), it is not surprising that the smoothed temperature trend in the United States box forced by them (Figure 7b) is very small over that period. The decrease in summertime surface temperature for the first few years in Figure 7a, even with an increasing full A1B forcing, is the result of interannual variability in regional climate. Ultimately, this variability is swamped by the increasing radiative forcing for both the full A1B scenario (Figure 7a) and the short-lived species (Figure 7b). The latter is driven by a drop in global sulfate loading (primarily over Asia) and the continued rise in BC (also primarily over Asia). We find that the summertime warming over the United States is significantly enhanced by projected changes in Asian emissions.

3.2. Precipitation and Soil Water

[34] In Figure 8, while the 21st century time series for global annual mean precipitation for both three-member ensembles show a modest increase of ~0.05 mm/d for both scenarios (only A1B is plotted) by year 2100, there is no statistically significant difference in their precipitation trends, as is evident in the plot of their difference. Unlike temperature, the largest changes in annual mean precipitation are over the ocean (up to 1 mm/d) and there is little difference between the hemispheres. As with temperature, the large-scale patterns in global, annual mean precipitation changes are similar for the full A1B scenario, the well-mixed greenhouse gases (A1B*), and the short-lived species (A1B − A1B*). However, unlike temperature, the patterns of precipitation changes driven by changes in short-lived species are, in general, not statistically significant.

[35] We now focus on the central United States (smaller box shown in Figure 5a). Our simulated 2100 decrease in JJA precipitation over the central United States for the full A1B scenario is qualitatively similar to the multimodel mean reported by the *IPCC* [2007a] and *Meehl et al.* [2007, Figure 10.9], though our decrease is larger. Moreover, we do find a statistically significant (at the 95% confidence level) decrease in 2100 precipitation relative to 2000 due to the change in radiative forcing from short-lived species (see the blue curves in Figure 9).

[36] We next consider root zone soil water, a quantity that integrates and responds to both temperature and precipitation. In Figure 9 we focus on the central United States

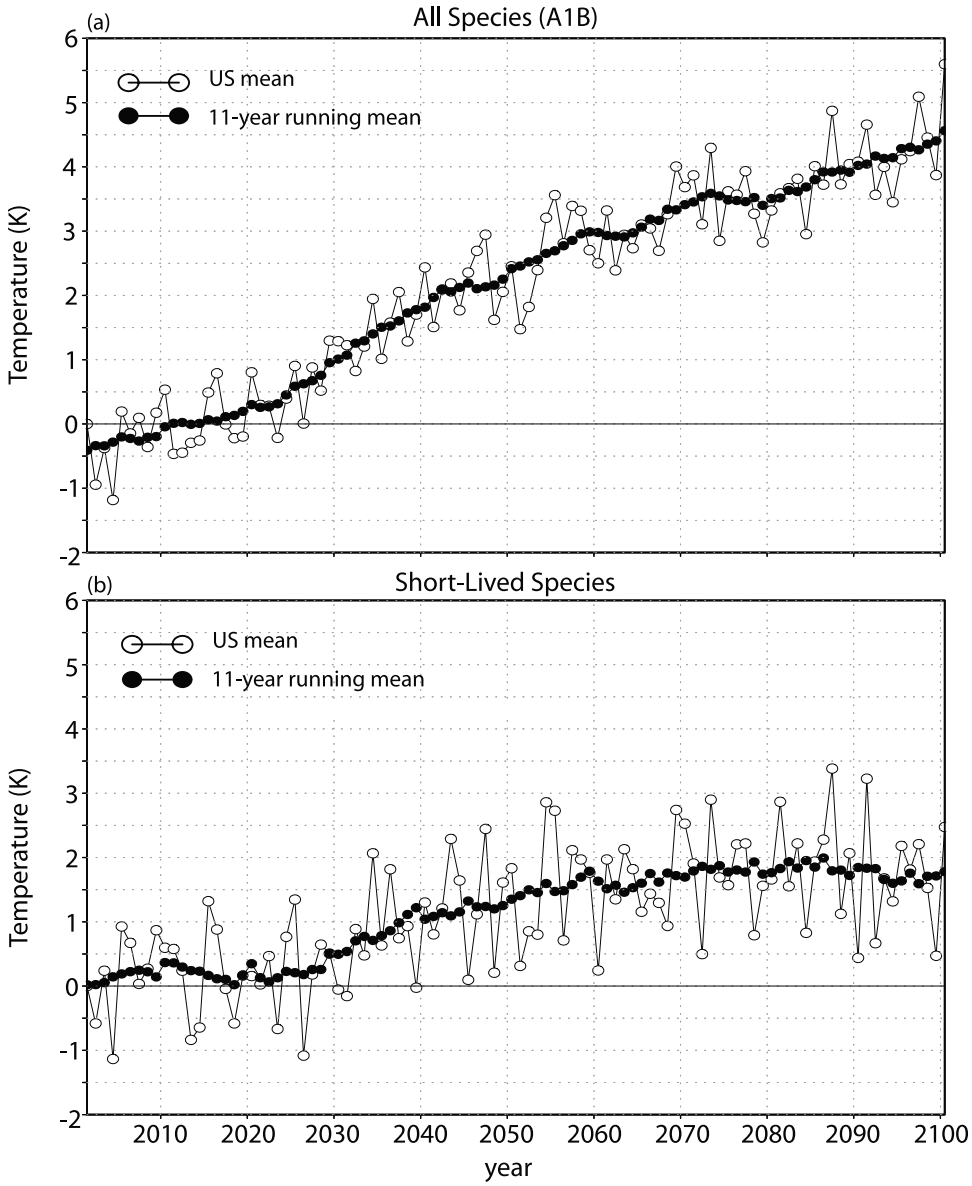

Figure 7. Time series of summer (JJA) average surface-air temperature changes (°K) relative to year 2001 for the continental United States (see the large box in Figure 5a) for the (a) full A1B scenario and (b) changes in short-lived species only (A1B − A1B*). The solid circles are the 11-year running mean.

where we show monthly mean area-averaged values of temperature, precipitation, and available root-zone soil water for both the full A1B scenario (dashed lines) and the A1B* scenario with short-lived species levels fixed at 2001 values (solid lines). The maximum root zone soil water (effectively the soil moisture bucket size; see *Milly and Shmakin* [2002] for details) is a spatially varying parameter dependent on the vegetation and soil type of each model grid box. Values are typically between 10 and 15 cm (100–150 kg/m^2).

[37] The values of temperature, precipitation, and available root zone soil water are ensemble averages over the last 40 years of the integrations. The qualitative results are not sensitive to the averaging period used, though 40 years gives better statistical significance. We have already identified a major impact of the A1B projected change in short-lived species (A1B − A1B*) on surface temperature (red curves) and a more modest impact on precipitation (blue curves). There is a statistically significant [at the 95% confidence level] decrease of up to 50% in available root zone soil water in the central United States during late summer (July–September). This is the result of a global increase in radiative forcing, located primarily over Asia, which in turn results from the large changes projected by the A1B scenario for Asian emissions of SO_2 and black carbon.

4. Summary

4.1. Major Results

[38] The major results of this study are as follows:

[39] 1. While changes in the levels of short-lived species projected by the A1B marker emission scenario have only modest impacts (5–10%) on global warming over the next 25 years, they strongly influence climate by the end of the

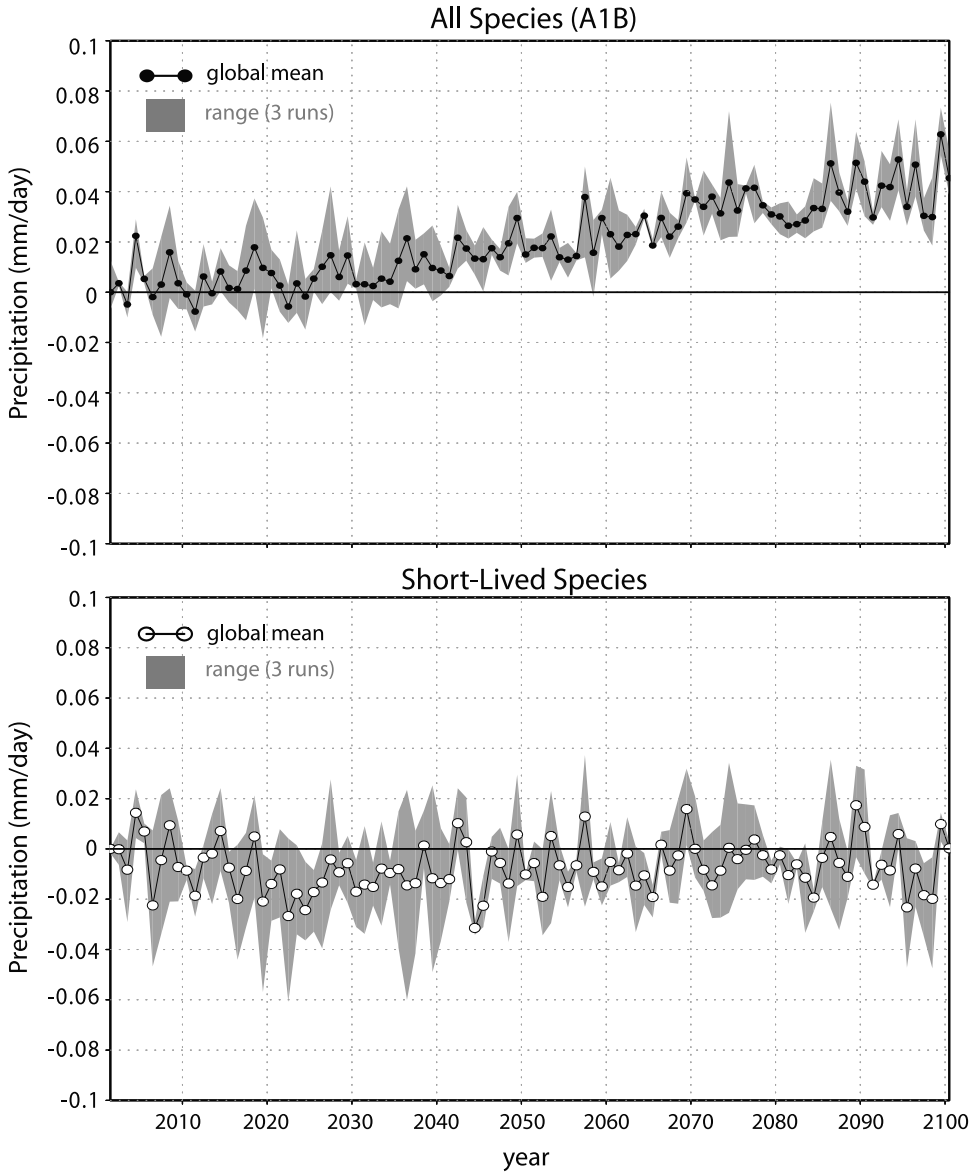

Figure 8. Annual average time series of global precipitation change (mm/d) relative to 2001 for the (a) A1B scenario and (b) short-lived species only (A1B − A1B*). The shaded area in Figure 8a represents the range of the three independent ensemble members, and in Figure 8b it represents the range of the three-ensemble pairs.

21st century (25% of the global warming and even more for the Northern Hemisphere).

[40] 2. By 2100, A1B marker scenario changes in global short-lived species emissions can contribute 40% of the summertime United States warming and enhance the wintertime NH high-latitude warming by 1.5–3°K.

[41] 3. The regional patterns of year 2100 warming are similar for the short-lived species and the well-mixed greenhouse gases and do not appear to be a direct local or regional climate response to local and regional patterns in emissions, loading, and radiative forcing. However, additional sensitivity tests employing a range of radiative forcings with different spatial distributions are needed to clearly identify the responsible mechanisms.

[42] 4. By 2100, 82% of the radiative forcing change relative to 2000 due to A1B marker scenario changes in short-lived species emissions is in the NH, and most of that is the result of a decrease in sulfate and increase in BC aerosol with only modest offsetting contributions from ozone and OC aerosol.

[43] 5. Considering the above results, we conclude that future climate studies must consider a suite of emission scenarios that while encompassing the full range of possible outcomes, treat the emissions of both the well-mixed greenhouse gases and the short-lived species consistently.

4.2. Uncertainties and Caveats

[44] The uncertainties still left after and caveats derived from this study are as follows:

[45] 1. Regional climate response patterns are model dependent [*Cubasch et al.*, 2001], though the major features that we simulate (strong winter warming in the Arctic and

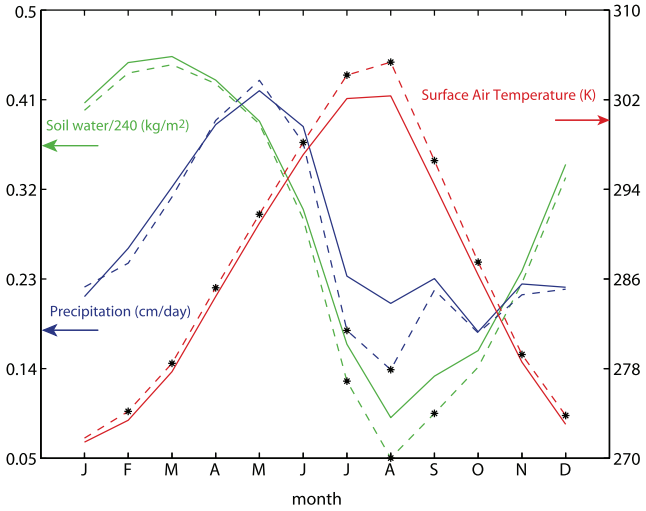

Figure 9. Monthly mean time series of available root zone soil water (green lines, in units of kg/m^2 scaled by a factor of 1/240 for plotting purposes on the left axis), precipitation (blue lines in cm/d on the left axis), and 2-m air temperature (red lines in °K on the right axis), averaged over the central United States (105–82.5°W longitude and 32.5–45°N latitude; see smaller box drawn on Figure 5a). Dashed lines are for the ensemble mean of the A1B experiments, averaged over the years 2061–2100; solid lines are for the ensemble mean of the A1B* experiments, averaged over the years 2061–2100. The stars represent those A1B monthly average values that are different from their companion A1B* values at the 95% confidence level.

the strong summer warming in the United States, southern Europe, and Mediterranean) are all robust features of the *IPCC* [2007a] multimodel mean for the A1B scenario [see *Meehl et al.*, 2007, Figure 10.9]. On the other hand, the climate in GFDL's climate model does have a summertime warm and dry bias over the United States' southern Great Plains [*Klein et al.*, 2006], and its simulated precipitation-minus-evaporation decrease in the southwestern United States for year 2100 of the A1B scenario is the most negative of the four climate models considered by *Seager et al.* [2007].

[46] 2. Almost all of the impacts of short-lived species on surface temperature, precipitation, and soil moisture by year 2100 are determined by end of the century emissions of all precursors, particularly SO_2 and black carbon. Currently, for a specific scenario or "storyline" such as A1B, there is a large quantitative spread and reasonable assumptions do not always even lead to the same sign for emissions trends projected out to 2100 for the short-lived species [e.g., *Shindell et al.* [2008]. The A1B marker scenario is only one of many "A1B" scenarios reported by SRES for a given storyline (e.g., *Shindell et al.* [2008]). Emissions of NO_x, black carbon, and organic carbon from biofuel and biomass burning are still uncertain and the assumption that black carbon emissions track carbon monoxide is problematical. Predicting emissions in the year 2100 requires not just enhanced scientific knowledge, but also the ability to predict social, economic, and technological developments and population trends 100 years into the future. Also there are still a number of ambiguities and uncertainties in current treatments of transport, deposition, and chemistry of short-lived species, in particular, sulfate aerosol and black carbon (see discussion by *Shindell et al.* [2008]).

[47] 3. This study does not include any indirect aerosol effects, though it is expected that the radiative forcing for the sulfate aerosol indirect effects will have the same sign as their direct effects [*Penner et al.*, 2001]. The radiative forcing for the aerosol indirect effect has been estimated to be at least equal to the direct effect, but with large uncertainty [*Forster et al.*, 2007]. The contribution of the semidirect cloud effect is also not specifically diagnosed. Aerosols are assumed to be externally mixed, which may affect both the radiative characteristics of the aerosols and their optical depth [*Jacobson*, 2001a, 2001b; *Shindell et al.*, 2008]. Surface albedo is held constant in time, thus omitting any effects on albedo due to increased black carbon deposition [*Hansen et al.*, 2007] or any other changes in the land surface.

[48] 4. In this study, we consider only the changes in ozone and aerosol concentrations caused by changes in anthropogenic emissions. Changes in these chemical species caused by climate change over the period 2000–2100 are neglected. Previous studies have generally concluded that climate change will tend to decrease tropospheric ozone concentrations by 5–15% over the next century, largely because of increased photochemical loss driven by higher humidity [e.g., *Brasseur et al.*, 2006; *Liao et al.*, 2006]. Other feedbacks that have been identified include changes in "natural" emissions (e.g., biomass burning, biogenic hydrocarbons, NO_x from lightning and soils, and dust), changes in stratosphere-troposphere exchange of ozone, and changes in rates of wet and dry deposition [e.g., *Zeng and Pyle*, 2003; *Stevenson et al.*, 2005; *Brasseur et al.*, 2006; *Liao et al.*, 2006]. These changes can lead to increased ozone concentrations in the tropics or near regions of high emissions of precursors and to either increased or decreased concentrations of aerosols. Methane is specified as a well-mixed greenhouse gas with prescribed concentrations in both the climate and chemical simulations, thus precluding any chemical feedbacks on methane concentrations via changes in atmospheric oxidant levels and methane lifetime [*Wild et al.*, 2001; *Fiore et al.*, 2002].

[49] **Acknowledgments.** We thank Ants Leetmaa for first suggesting this study, Ron Stouffer, Tom Delworth, and Tom Knutson for their comments and advice, and two anonymous reviewers for their thorough and thoughtful reviews.

References

Alley, et al. (2007), Summary for policymakers, in *Climate Change 2007: The Physical Science Basis: Contribution of Working Group I to the Fourth Assessment Report of the Intergovernmental Panel on Climate Change*, edited by S. Solomon et al., pp. 996, Cambridge Univ. Press, New York.

Boer, G. J., and B. Yu (2003), Climate sensitivity and response, *Clim. Dyn.*, *20*, 415–419.

Brasseur, G. P., and E. Roeckner (2005), Impact of improved air quality on the future evolution of climate, *Geophys. Res. Lett.*, *32*, L23704, doi:10.1029/2005GL023902.

Brasseur, G. P., M. Schultz, C. Granier, M. Saunois, T. Diehl, M. Botzet, E. Roeckner, and S. Walters (2006), Impact of climate change on the future chemical composition of the global troposphere, *J. Clim.*, *19*, 3932–3951.

Bryson, R. A., and G. J. Dittberner (1976), A non-equilibrium model of hemispheric mean surface temperature, *J. Atmos. Sci.*, *33*, 2094–2106.

Cubasch, U., et al. (2001), Projections of future climate change, in *Climate Change 2001: The Scientific Basis: Contribution of Working Group I to the Third Assessment Report of the Intergovernmental Panel on Climate Change*, edited by J. T. Houghton et al., pp. 526–582, Cambridge Univ. Press, New York.

Delworth, T. L., et al. (2006), GFDL's CM2 global coupled climate models: part I: Formulation and simulation characteristics, *J. Clim.*, *19*(5), 643–674.

Fiore, A. M., D. J. Jacob, B. D. Field, D. G. Streets, S. D. Fernandes, and C. Jang (2002), Linking ozone pollution and climate change: The case for controlling methane, *Geophys. Res. Lett.*, *29*(19), 1919, doi:10.1029/2002GL015601.

Forster, P., M. Blackburn, R. Glover, and K. Shine (2000), An examination of climate sensitivity for idealized climate change experiments in an intermediate general circulation model, *Clim. Dyn.*, *16*, 833–849.

Forster, P., et al. (2007), Changes in atmospheric constituents and radiative forcing, in *Climate Change 2007: The Physical Science Basis: Contribution of Working Group I to the Fourth Assessment Report of the Intergovernmental Panel on Climate Change*, edited by S. Solomon et al., pp. 129–234, Cambridge Univ. Press, New York.

Ginoux, P., L. W. Horowitz, V. Ramaswamy, I. V. Geogdzhayev, B. N. Holben, G. Stenchikov, and X. Tie (2006), Evaluation of aerosol distribution and optical depth in the Geophysical Fluid Dynamics Laboratory coupled model CM2.1 for present climate, *J. Geophys. Res.*, *111*, D22210, doi:10.1029/2005JD006707.

Hansen, J., M. Sato, R. Ruedy, A. Lacis, and V. Oinas (2000), Global warming in the twenty-first century: An alternative scenario, *Proc. Natl. Acad. Sci. U. S. A.*, *97*, 9875–9880, doi:10.1073/pnas.170278997.

Hansen, J., M. Sato, P. Kharecha, G. Russell, D. W. Lea, and M. Siddall (2007), Climate change and trace gases, *Philos. Trans. R. Soc. London Ser. A*, *365*, 1925–1954, doi:10.1098/rsta.2007.2052.

Haywood, J. M., V. Ramaswamy, and B. J. Soden (1999), Tropospheric aerosol climate forcing in clear-sky satellite observations over the oceans, *Science*, *283*(5406), 1299–1303.

Horowitz, L. W. (2006), Past, present, and future concentrations of tropospheric ozone and aerosols: Methodology, ozone evaluation, and sensitivity to aerosol wet removal, *J. Geophys. Res.*, *111*, D22211, doi:10.1029/2005JD006937.

Horowitz, L. W., et al. (2003), A global simulation of tropospheric ozone and related tracers: Description and evaluation of MOZART, version 2, *J. Geophys. Res.*, *108*(D24), 4784, doi:10.1029/2002JD002853.

Intergovernmental Panel on Climate Change (2001), *Climate Change 2001: The Physical Science Basis*, edited by J. T. Houghton et al., 881 pp., Cambridge Univ. Press, New York.

Intergovernmental Panel on Climate Change (2007a), Summary for policymakers, in *Climate Change 2007: The Physical Science Basis: Contribution of Working Group I to the Fourth Assessment Report of the Intergovernmental Panel on Climate Change*, 21 pp., edited by S. Solomon et al., Cambridge Univ. Press, New York.

Intergovernmental Panel on Climate Change (2007b), *Climate Change 2007: The Physical Science Basis: Contribution of Working Group I to the Fourth Assessment Report of the Intergovernmental Panel on Climate Change*, edited by S. Solomon et al., 996 pp., Cambridge Univ. Press, New York.

Jacobson, M. Z. (2001a), Global direct radiative forcing due to multicomponent anthropogenic and natural aerosols, *J. Geophys. Res.*, *106*(D2), 1551–1568.

Jacobson, M. Z. (2001b), Strong radiative heating due to the mixing state of black carbon in atmospheric aerosols, *Nature*, *409*, 695–697, doi:10.1038/35055518.

Kiehl, J. T., J. J. Hack, G. B. Bonan, B. A. Boville, D. L. Williamson, and P. J. Rasch (1998), The National Center for Atmospheric Research Community Climate Model: CCM3, *J. Clim.*, *11*, 1131–1149.

Klein, S. A., X. Jiang, J. Boyle, S. Malyshev, and S. Xie (2006), Diagnosis of the summertime warm and dry bias over the U.S. Southern Great Plains in the GFDL climate model using a weather forecasting approach, *Geophys. Res. Lett.*, *33*, L18805, doi:10.1029/2006GL027567.

Knutson, T. R., T. L. Delworth, K. W. Dixon, I. M. Held, J. Lu, V. Ramaswamy, M. D. Schwarzkopf, G. Stenchikov, and R. J. Stouffer (2006), Assessment of twentieth-century regional surface temperature trends using the GFDL CM2 coupled models, *J. Clim.*, *10*(9), 1624–1651.

Liao, H., W.-T. Chen, and J. H. Seinfeld (2006), Role of climate change in global predictions of future tropospheric ozone and aerosols, *J. Geophys. Res.*, *111*, D12304, doi:10.1029/2005JD006852.

Meehl, G. A., et al. (2007), Global climate projections, in *Climate Change 2007: The Physical Science Basis: Contribution of Working Group I to the Fourth Assessment Report of the Intergovernmental Panel on Climate Change*, edited by S. Solomon et al., pp. 747–845, Cambridge Univ. Press, New York.

Milly, P. C. D., and A. B. Shmakin (2002), Global modeling of land water and energy balances: part I: The land dynamics (LaD) model, *J. Hydrometeorol.*, *3*(3), 283–299.

Mitchell, J. F. B., et al. (2001), Detection of Climate Change and Attribution of Causes: Contribution of working group I to the third assessment report of the Intergovernmental Panel on Climate Change, in *Climate Change 2001: The Scientific Basis*, edited by J. T. Houghton et al., pp. 526–582, Cambridge Univ. Press, New York.

Nakicenovic, N., and R. Swart (Eds.) (2000), *Special Report on Emissions Scenarios: A Special Report of Working Group III of the Intergovernmental Panel on Climate Change*, 599 pp., Cambridge Univ. Press, New York.

Penner, J. E., et al. (2001), Aerosols, their direct and indirect effects, in *Climate Change 2001: The Scientific Basis: Contribution of Working Group I to the Third Assessment Report of the Intergovernmental Panel on Climate Change*, edited by J. T. Houghton et al., pp. 289–348, Cambridge Univ. Press, Cambridge, U.K.

Ramaswamy, V., et al. (2001), Radiative forcing of climate change, in *Climate Change 2001: The Scientific Basis: Contribution of Working Group I to the Third Assessment Report of the Intergovernmental Panel on Climate Change*, edited by J. T. Houghton et al., pp. 349–416, Cambridge Univ. Press, Cambridge, U.K.

Schimel, D., et al. (1996), Radiative forcing of climate change, in *Climate Change 1995: The Science of Climate Change*, edited by J. T. Houghton et al., 572 pp., Cambridge Univ. Press, New York.

Seager, R., et al. (2007), Model projections of an imminent transition to a more arid climate in southwestern North America, *Science*, *316*(5828), 1181–1184.

Shindell, D. T., H. Levy, M. D. Schwarzkopf, L. W. Horowitz, J. F. Lamarque, and G. Faluvegi (2008), Multi-model projections of climate change from short-lived emissions due to human activities, *J. Geophys. Res.*, doi:10.1029/2007JD009152, in press.

Shine, K. P., et al. (1990), Radiative forcing of climate, in *Climate Change: The IPCC Scientific Assessment*, edited by J. T. Houghton, G. J. Jenkins, and J. J. Ephraums, 365 pp., Cambridge Univ. Press, New York.

Shine, K. P., et al. (1995), Radiative forcing, in *Climate Change 1994: Radiative Forcing of Climate Change and An Evaluation of the IPCC IS92 Emission Scenarios*, edited by J. T. Houghton et al., 339 pp., Cambridge Univ. Press, New York.

Stevenson, D., R. Doherty, M. Sanderson, C. Johnson, B. Collins, and D. Derwent (2005), Impacts of climate change and variability on tropospheric ozone and its precursors, *Faraday Discuss.*, *130*, 41–57, doi:10.1039/b417412g.

Stouffer, R. J., et al. (2006), GFDL's CM2 global coupled climate models: part IV: Idealized climate response, *J. Clim.*, *19*(5), 723–740.

Tie, X., S. Madronich, S. Walters, D. P. Edwards, P. Ginoux, N. Mahowald, R. Zhang, C. Lou, and G. Brasseur (2005), Assessment of the global impact of aerosols on tropospheric oxidants, *J. Geophys. Res.*, *110*, D03204, doi:10.1029/2004JD005359.

Wetherald, R. T., and S. Manabe (1980), Cloud cover and climate sensitivity, *J. Atmos. Sci.*, *37*(7), 1485–1510.

Wild, O., M. J. Prather, and H. Akimoto (2001), Indirect long-term global radiative cooling from NO_x emissions, *Geophys. Res. Lett.*, *28*(9), 1719–1722.

Wittenberg, A. T., A. Rosati, N.-C. Lau, and J. J. Ploshay (2006), GFDL's CM2 global coupled climate models: part III: Tropical Pacific climate and ENSO, *J. Clim.*, *19*(5), 698–722.

Zeng, G., and J. A. Pyle (2003), Changes in tropospheric ozone between 2000 and 2100 modeled in a chemistry-climate model, *Geophys. Res. Lett.*, *30*(7), 1392, doi:10.1029/2002GL016708.

K. L. Findell, L. Horowitz, H. Levy II, V. Ramaswamy, and M. D. Schwarzkopf, Geophysical Fluid Dynamics Laboratory, NOAA, Princeton University, P.O Box 308, Princeton, NJ 08542, USA. (hiram.levy@noaa.gov)